CHEMISTRY
A EUROPEAN JOURNAL

DOI: 10.1002/chem.200601854

# Supramolecular Triad and Pentad Composed of Zinc–Porphyrin(s), Oxoporphyrinogen, and Fullerene(s): Design and Electron-Transfer Studies

**Amy Lea Schumacher,[a] Atula S. D. Sandanayaka,[b] Jonathan P. Hill,*[c] Katsuhiko Ariga,[c] Paul A. Karr,[a] Yasuyuki Araki,[b] Osamu Ito,*[b] and Francis D'Souza*[a]**

**Abstract:** By adopting a "covalent–coordinate" bonding approach, novel supramolecular pentad and triad molecules composed of zinc–porphyrin(s), fullerene(s), and oxoporphyrinogen redox-/photoactive entities have been constructed, and also characterized by means of spectral and electrochemical techniques. The geometry and electronic structures of the pentad and the triad were deduced by means of DFT calculations. Free-energy calculations suggested that the photoinduced electron/energy transfer from the zinc–porphyrin (ZnP) singlet-excited state to the imidazole modified fullerene ($ImC_{60}$) acceptor and oxoporphyrinogen (OxP) entities is feasible for both the triad and the pentad. The charge-separation rates ($k_{CS}$) determined from picosecond time-resolved emission studies were higher for pentad $(C_{60}Im{:}ZnP)_2$–OxP than for the corresponding triad, $C_{60}Im{:}ZnP$–OxP. A comparison of the $k_{CS}$ values previously reported for the covalently linked bis-(zinc–porphyrin)–oxoporphyrinogen triad suggests that employing a fullerene acceptor improves the electron-transfer rates. Nanosecond transient absorption studies provide evidence for the occurrence of electron-transfer processes. Lifetimes of the radical ion pairs ($\tau_{RIP}$) are in the range of hundreds of nanoseconds, which indicates that there is charge stabilization in the supramolecular systems.

**Keywords:** density functional calculations · electron transfer · fullerenes · porphyrinoids · supramolecular chemistry

## Introduction

Energy- and electron-transfer processes in molecular and supramolecular donor–acceptor systems are of current interest 1) to address the mechanistic details of electron transfer in chemistry and biology,[1–3] 2) to develop light-energy harvesting systems,[4–8] and 3) to build optoelectronic devices.[9] To achieve these goals, elegantly designed covalently linked donor–acceptor systems are frequently employed, whereas self-assembled donor–acceptor systems have been utilized in few studies.[10] Developments in molecular/supramolecular polyads (triads, tetrads, pentads, etc.) have recently stimulated interest owing to applications in generating long-lived, charge-separated states through the charge migration route, and for the construction of systems that are capable of performing "antenna-reaction center" processes.[10–12] To construct these novel systems, porphyrins, phthalocyanines, or ruthenium(II) tris(bipyridine) are often used as primary electron donors, whereas fullerene, quinone, nitroaromatic compounds, metal complexes, or pyromellitic anhydride have been used as electron acceptors.[10–12] Electron donors like ferrocene, amines, and tetrathiafulvalenes are employed

[a] A. L. Schumacher, Prof. P. A. Karr, Prof. F. D'Souza
Department of Chemistry
Wichita State University
1845 Fairmount, Wichita, Kansas 67260–0051 (USA)
Fax: (+1) 316-978-3431
E-mail: Francis.DSouza@wichita.edu

[b] Dr. A. S. D. Sandanayaka, Dr. Y. Araki, Prof. O. Ito
Institute of Multidisciplinary Research for Advanced Materials
Tohoku University
Katahira, Aoba-ku, Sendai, 980-8577 (Japan)
Fax: (+81) 22-217-5610
E-mail: ito@tagen.tohoku.ac.jp

[c] Dr. J. P. Hill, Prof. K. Ariga
Supermolecules Group
National Institute for Materials Science
Namiki 1-1, Tsukuba 305-0044, Ibaraki (Japan)
Fax: (+81) 29-860-4832
E-mail: Jonathan.hill@nims.go.jp

Supporting information for this article is available on the WWW under http://www.chemeurj.org/ or from the author.

as secondary electron donors to build these polyads.[11–12] Furthermore, fluorophores, such as boron dipyrrin and anthracene, have been used to create the antenna functionality.[10–12] Among the electron acceptors, fullerenes[13] have drawn special attention as a result of their three-dimensional structure, their similar reduction potentials to benzoquinone, their absorption spectra, which extend over most of the visible spectral region, and their small reorganization energy in electron-transfer reactions.[14] Consequently, many covalently linked, self-assembled donor–acceptor systems[11–12] that contain fullerenes have been reported.

Recently, we reported details of a porphyrin–quinonoid donor–acceptor triad that featured two zinc–porphyrins (ZnPs) covalently attached to an oxoporphyrinogen (OxP) through its macrocyclic nitrogen atoms.[15] Time-resolved fluorescence studies of the ZnP–OxP dyad and the triad ($(ZnP)_n$–OxP; $n=1$ and 2, respectively) revealed that there was excited-state energy transfer from the zinc–porphyrin to the oxoporphyrinogen in nonpolar solvents. However, in polar solvents nanosecond transient absorption studies indicated the occurrence of photoinduced charge separation from the ZnP singlet-excited state to OxP. In seeking donor–acceptor systems that result in improved charge separation, we have constructed a supramolecular triad and also a pentad that feature functionalized fullerene(s) and $(ZnP)_n$–OxP by using the "covalent–coordinate" bonding approach. For the triad, the ZnP–OxP dyad was axially coordinated to $ImC_{60}$ (1 equiv) to yield ($C_{60}$Im:ZnP)–OxP. For the pentad, $ImC_{60}$ (2 equiv) was axially coordinated to the zinc center of covalently linked $(ZnP)_2$–OxP to yield pentad $(C_{60}Im:ZnP)_2$–OxP. For comparative purposes, dyad $C_{60}$Im:ZnP was also constructed. In the pentad and the triad, competition is expected between electron transfer to either $C_{60}$ or OxP from the ZnP singlet-excited state. The present investigation shows that the overall charge-separation process between ZnP and $C_{60}$ is accelerated when $C_{60}$ is present in the triad or the pentad.

## Results and Discussion

The optical absorption spectrum of the newly synthesized ZnP–OxP dyad contains bands at $\lambda=424$ and 546 nm, which correspond to the ZnP entity, and a band at $\lambda=511$ nm, which corresponds to the OxP entity in *o*-dichlorobenzene (DCB). Similar spectral features were also observed for the $(ZnP)_2$–OxP triad. However, the intensity of the ZnP bands was double that observed for the ZnP–OxP dyad because two ZnP macrocycles are present.[15] Coordinative supramolecular assembly with $ImC_{60}$ was monitored by using optical absorption methods.[16] Figure 1 shows the spectral changes observed upon the addition of $ImC_{60}$ to a solution of ZnP–OxP in DCB. Spectral changes include a redshift of the ZnP Soret band accompanied by a decrease in its inten-

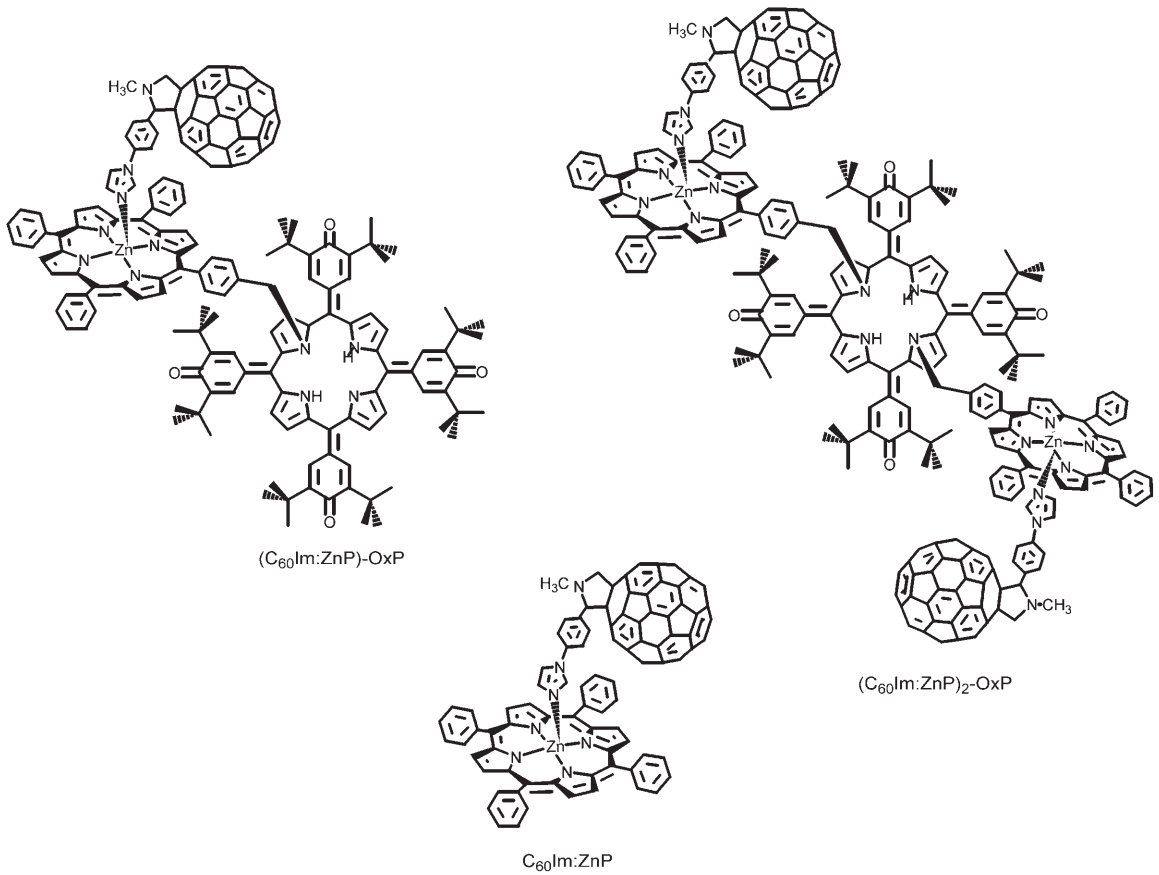


  

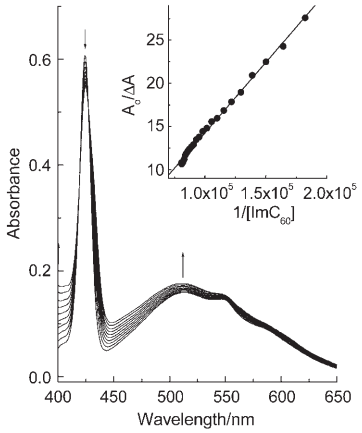


Figure 1. UV-visible spectral changes observed during the titration of $ImC_{60}$ (1.3 μM each addition) with ZnP–OxP (2.0 μM) in *o*-dichlorobenzene (DCB). The inset shows a Benesi–Hildebrand plot constructed to evaluate the binding constant. $A_o$ is the intensity observed in the absence of $ImC_{60}$ and $\Delta A$ is the change in absorption upon the addition of $ImC_{60}$.

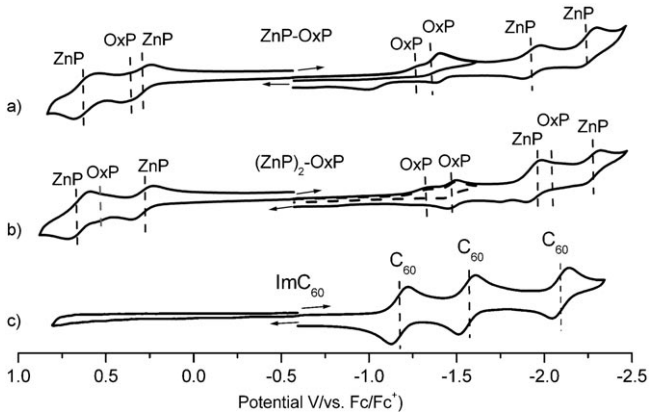


Figure 2. Cyclic voltammograms of ZnP–OxP (a), $(ZnP)_2$–OxP (b), and $ImC_{60}$ (c) in DCB, which contains $(n\text{Bu})_4\text{NClO}_4$ (0.1 M). Scan rate = 100 mV $s^{-1}$.

sity. Isosbestic points at $\lambda = 419$ and 427 nm were observed that suggest the existence of one equilibrium process in solution. During the titration, the band at $\lambda = 511$ nm, which corresponds to OxP, revealed no changes in the absorption maxima, and indicates that there is a lack of interaction between the OxP and the $ImC_{60}$ entities. A Job's plot constructed from spectral data indicated 1:1 complexation, which confirms the formation of the ($C_{60}$Im:ZnP)–OxP triad. The formation constant calculated from a Benesi–Hildebrand plot[17] was $1.26\times10^4\,M^{-1}$ in DCB (Figure 1 inset), which is comparable to a value of $1.16\times10^4\,M^{-1}$ for the dyad in DCB,[16] and reasonably suggests the formation of a stable complex.

Titration of $(ZnP)_2$–OxP with $ImC_{60}$ revealed spectral changes similar to those observed for the triad (See the Supporting Information). Namely, a red-shifted ZnP Soret band and one or more isosbestic points were observed. A Job's plot confirmed 1:2 stoichiometry to establish the formation of pentad $(C_{60}Im:ZnP)_2$–OxP in solution.

**Electrochemistry**: Electrochemical studies were performed to evaluate the redox potentials of the individual entities and the energetics of different photochemical processes. Figure 2 shows the cyclic voltammograms of $(ZnP)_n$–OxP and $ImC_{60}$ in DCB, which contains $(n\text{Bu})_4\text{NClO}_4$ (0.1 M). Owing to the presence of multiple redox-active entities, the voltammograms of $(ZnP)_n$–OxP are complex. However, accurate analysis of the site of electron transfer that corresponds to the individual redox entities was possible by comparing the voltammograms of ZnP with those of mono and bis methylenenaphthyl N-substituted porphyrinogens.[18] The site of electron transfer thus obtained is indicated at the top of each redox couple. For $(ZnP)_n$–OxP, the redox potentials measured for the ZnP entities are close to those obtained for reference compound ZnP (two one-electron oxidations at 0.28 and 0.62 V versus $Fc/Fc^+$, and two one-electron reductions at −1.92 and −2.23 V versus $Fc/Fc^+$), which suggests the absence of interactions between ZnP and OxP units. The redox potentials that correspond to the oxidation and reduction of the OxP entity are close to their respective N-alkylated analogues. The first reversible oxidations of OxP are located at 0.37 V and 0.47 V, whereas the first reductions for ZnP–OxP and $(ZnP)_2$–OxP are located at $E_{pc} = -1.29$ and $E_{pc} = -1.36$ V, respectively. The more facile reduction of the OxP entity (analogous with quinones electron acceptors) in $(ZnP)_n$–OxP suggests that it should act as an electron acceptor. The HOMO–LUMO gaps, measured as the potential difference between the first oxidation of the ZnP donor entity and the OxP acceptor entity for (ZnP–OxP) and $(ZnP)_2$–OxP, were found to be −1.57 and 1.61 V, respectively.

In the supramolecular assemblies described, the first three one-electron reductions of $ImC_{60}$ were located at $E_{1/2} = -1.13$, −1.51, and −2.05 V versus $Fc/Fc^+$. There is no significant shift (< 10 mV) in potential upon coordination of $ImC_{60}$ to the ZnP moieties of $(ZnP)_n$–OxP. The HOMO-(ZnP)–LUMO($ImC_{60}$) gap for $(C_{60}Im:ZnP)_n$–OxP was found to be 1.40 V from experimental results, which is similar to that of the dyad (1.41 V). Thus, the smaller HOMO–LUMO gap of ($C_{60}$Im:ZnP)–OxP indicates that the charge-separated state $(ZnP^{\bullet+}:ImC_{60}^{\bullet-})$–OxP is more stable than $(ZnP^{\bullet+}:ImC_{60})$–$OxP^{\bullet-}$; this situation is the same for the pentad. The free-energy changes of charge separation, $\Delta G_{CS}$, were calculated according to the Rehm–Weller approach[19] by using the first oxidation potential of ZnP, the first reduction potential of OxP or $C_{60}$, the singlet excitation energy of ZnP, and the estimated Coulomb energy. The $\Delta G^Z_{CS}$ values for generating radical ion pairs (RIP) $ZnP^{\bullet+}$–$OxP^{\bullet-}$ and $(ZnP)(ZnP^{\bullet+})$–$OxP^{\bullet-}$ measured in DCB were −0.63 and −0.58 eV, respectively, which indicates the possibility of photoinduced charge separation from the ZnP singlet-excited state to the OxP entity. Similar calculations performed on $(ZnP:ImC_{60})_n$–OxP resulted in a $\Delta G^Z_{CS}$ value of −0.73 eV for both $n = 1$ and 2, which indicates that a more exothermic charge separation process from the ZnP singlet-excited state to the $C_{60}$ entity occurs in DCB.

  

**DFT B3LYP/3-21G(*) studies**: To understand the structure of the triad and the pentad, computational calculations were performed at the B3LYP/3-21G(*) level.[20–21] Starting molecules $ImC_{60}$ and $(ZnP)_n$–OxP were fully optimized to a stationary point on the Born–Oppenheimer potential energy surface and allowed to interact. Figure 3 shows the optimized structures of the supramolecular complexes. It should be mentioned here that owing to the very flexible nature of the systems, several structures are plausible, but those shown in Figure 3 appear to be the lowest energy structures. In agreement with earlier X-ray and computational analyses of bis N-alkyl substituted oxoporphyrinogens,[18] the oxoporphyrinogen in optimized $(C_{60}Im{:}ZnP)_n$–OxP has a highly ruffled structure, in which the β-pyrrole carbon is displaced by as much as 1.7 Å. Additionally, based on $^1$H NMR spectral data, the two zinc–porphyrin units in $(ZnP)_2$–OxP were assumed to be the *cis*-isomeric form, that is, pointing in the same direction with respect to the plane of OxP macrocycle. In the optimized structure of $(C_{60}Im{:}ZnP)_2$–OxP, the Zn–Zn distance between the two ZnP moieties was ≈19 Å, whereas the distance between Zn and the center of OxP was ≈12 Å. The two fullerene entities were separated by as much as 29 Å, whereas the closest center-to-center distance between ZnP and $C_{60}$ was ≈13 Å. For $(C_{60}Im{:}ZnP)_n$–OxP, the center-to-center distance between ZnP and $C_{60}$ was ≈13.7 Å, whereas the distance between OxP and $C_{60}$ was ≈15 Å. Thus, no apparent association between the different entities was observed for $(C_{60}Im{:}ZnP)_n$–OxP ($n=1$ and 2), which is in agreement with the optical absorption data discussed earlier.

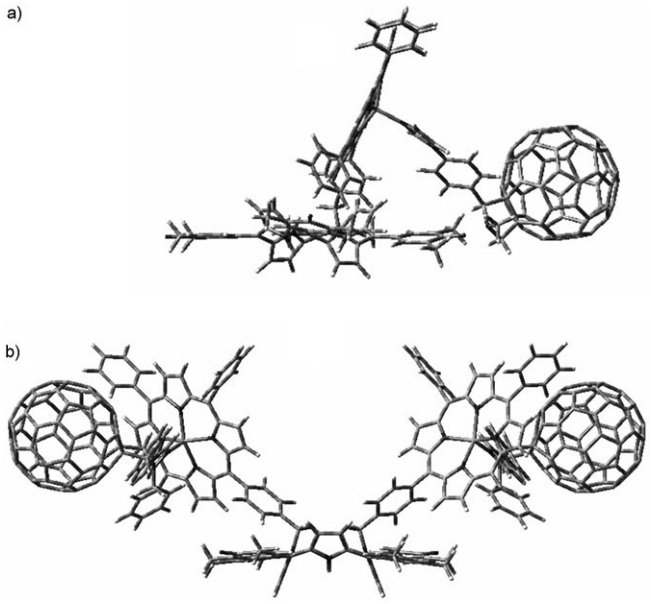


Figure 3. B3LYP/3-21G(*) optimized structure of the $(C_{60}Im{:}ZnP)$–OxP triad (a) and the $(C_{60}Im{:}ZnP)_2$–OxP pentad (b).

The HOMO(ZnP)–LUMO($C_{60}$) values for $(C_{60}Im{:}ZnP)_n$–OxP ($n=1$ and 2) calculated by using B3LYP/3-21G(*) in the gas phase were found to be 1.02 and 0.99 eV, respectively. These values are lower than those obtained from electrochemical data, a trend that was also reported for triad $C_{60}Im{:}ZnP$.[16]

**Photochemical studies**: The emission behavior of the supramolecular systems was initially investigated by using steady-state fluorescence, and subsequently by means of time-resolved emission and transient absorption methods. Figure 4a shows the emission spectrum of ZnP and $(ZnP)_n$–OxP in DCB. The intensities of the ZnP emission bands located at $\lambda=600$ and 646 nm were quenched by >85% for ZnP–OxP and by >95% for $(ZnP)_2$–OxP. In addition to ZnP emission bands, there was also a weak emission band at $\lambda=720$ nm that corresponds to the N-substituted porphyrinogen moeity in both derivatives, and was confirmed by means of independent experiments performed with simple N-alkylated porphyrinogens.

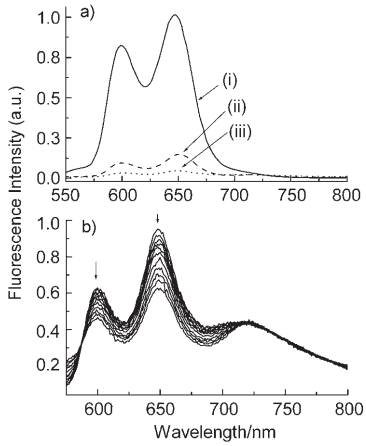


Figure 4. a) Fluorescence spectrum of ZnP (i), ZnP–OxP (ii), and $(ZnP)_2$–OxP (iii) in DCB. The samples were excited at the Soret band position of ZnP and the concentrations of the compounds were held at 10 μM. b) Changes in the fluorescence spectra observed upon the addition of increasing concentrations of $ImC_{60}$ (5 μM each addition) to a solution of $(ZnP)_2$–OxP in DCB.

As shown in Figure 4b, addition of $ImC_{60}$ to a solution of $(ZnP)_n$–OxP in DCB causes additional quenching of the ZnP emission bands, and confirms the interaction between $C_{60}Im$ and ZnP owing to the formation of a supramolecular pentad or a triad. Because of the observed decrease in ZnP emission intensities, the occurrence of one or both of the following processes is suggested: 1) charge-separation quenching from the singlet-excited state of ZnP to the fullerene entity and 2) energy transfer from ZnP to the fullerene entity. In the following sections, the time-resolved emission spectral results are discussed to verify the different quenching pathways.

Emission from pristine ZnP shows a monoexponential decay when it is dissolved in either toluene or DCB. As recently documented,[15] the ZnP emissions in $(ZnP)_n$–OxP were quenched and follow a biexponential decay with major short and minor long components. The lifetime of the minor

  

long component is comparable to that of unbound ZnP (see Table 1). From the major short decay component of $^1$ZnP* (fluorescence lifetime is defined as $\tau_f^Z$), the quenching rate ($k_q$) and quantum yield ($\Phi_q$) calculated for the dyad and the triad were $\approx 1.0\times10^{10}$ s$^{-1}$ and $>0.95$, respectively (see footnote [a] in Table 1 for relevant equations). In nonpolar solvents, such as toluene, the fluorescence quenching process can be mainly attributed to energy transfer owing to an insufficient driving force for the charge-separation process ($\Delta G_{CS}^Z = -0.05$ eV in Table 1). In slightly polar DCB, the results indicate that photoinduced charge separation from $^1$ZnP* to OxP occurs, as revealed in our previous paper.[15]

Addition of ImC$_{60}$ to (ZnP)$_n$–OxP forms the supramolecular structure (C$_{60}$Im:ZnP)$_n$–OxP, which causes additional quenching of the ZnP emission (Figure 5). For the pentad, the lifetime of ZnP was $\tau_f^Z = <10$ ps, which is close to the time resolution of our instrument. The lifetime of the quenched component of ZnP in (C$_{60}$Im:ZnP)–OxP was $\tau_f^Z =$ 79 ps in DCB; that is, highly efficient quenching was observed in both the supramolecular triad and the pentad. The photophysical data are given in Table 1. Increasing the polarity of the solvent led to acceleration of the quenching of the ZnP singlet-excited state based on the increase in the negative free-energy change ($\Delta G_{CS}^Z = -0.73$ eV in DCB); this observation has been interpreted in terms of the occurrence of a competitive charge-separation process from $^1$ZnP* to the C$_{60}$ moiety.

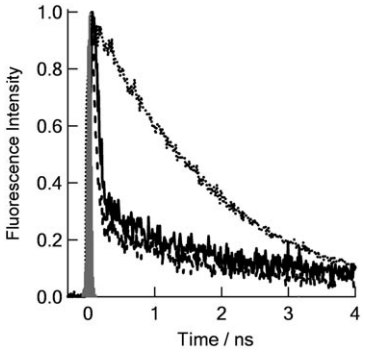


Figure 5. Fluorescence decay profiles for ZnP–OxP (0.07 mM) and (C$_{60}$Im:ZnP)–OxP (+[C$_{60}$Im] = 0.07 mM) measured in the $\lambda = 600$–640 nm region, which corresponds to zinc–porphyrin emission in DCB: •••••, (tetraphenylporphyrinato)zinc(II) in toluene; ——, C$_{60}$Im:ZnP–OxP in toluene; – – –, C$_{60}$Im:ZnP–OxP in DCB.

The fluorescence–time profiles in the $\lambda = 700$–750 nm region in toluene and DCB were also monitored for (C$_{60}$Im:ZnP)$_n$–OxP (Figure 6). Both C$_{60}$ and OxP emit in this wavelength region. The fluorescence lifetimes $\tau_f^{C,O}$, evaluated by using a curve fitting method, are listed in Table 1. In DCB, the $\tau_f^{C,O}$ values are 160 and 100 ps for (C$_{60}$Im:ZnP)$_n$–OxP in which $n = 1$ and 2, respectively. From these $\tau_f^{C,O}$ values, the rate constants ($k_q^{C,O}$) and quantum yields ($\Phi_q^{C,O}$) were evaluated and are summarized in Table 1. The $k_q^{C,O}$ values are in the range of $(4.0$–$8.0)\times10^9$ s$^{-1}$ and the

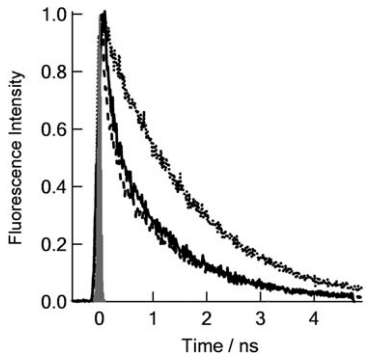


Figure 6. Fluorescence decay profiles of (C$_{60}$Im:ZnP)$_2$–OxP ([component] = 0.07 mM) collected in the 700–750 nm corresponding to C$_{60}$ emission in DCB, $\lambda_{ex} = 410$ nm: •••••, ImC$_{60}$ in toluene; ——, (C$_{60}$Im:ZnP)$_2$–OxP in toluene; – – –, (C$_{60}$Im:ZnP)$_2$–OxP in DCB.

Table 1. The photophysical data for the compounds studied herein.

| Compound | Solvent | $\tau_f^Z$ [ps][a] $^1$ZnP* | $k_q^{Z[a]}$ [s$^{-1}$] $^1$ZnP* | $\Phi_q^{Z[a]}$ $^1$ZnP* | $-\Delta G_{CS}^{Z}$ [b] [eV] | $\tau_f^{C,O}$ [ps][a] $^1$C$_{60}$* | $k_q^{C,O[a]}$ [s$^{-1}$] $^1$C$_{60}$* | $\Phi_q^{C,O[a]}$ $^1$C$_{60}$* | $-\Delta G_{CS}^{C}$ [b] [eV] | $k_{CS}$ [c,d] [s$^{-1}$] | $\tau_{RIP}$ [e] [ns] |
|---|---|---|---|---|---|---|---|---|---|---|---|
| ZnP–OxP | DCB | 102 | $9.3\times10^9$ | 0.95 | 0.65[f] | 50 ($\tau_f^O$) | | | | | |
| | toluene | 147 | $6.3\times10^9$ | 0.93 | – | 56 ($\tau_f^O$) | | | | | |
| (C$_{60}$Im:ZnP)–OxP | DCB | 79 | $1.2\times10^{10}$ | 0.96 | 0.73[f] (0.66)[g] | 100 ($\tau_f^C$) | $9.3\times10^9$ | 0.93 | 0.34[g] | $9.5\times10^6$ (1020 nm) | 110 |
| | toluene | 92 | $1.0\times10^{10}$ | 0.95 | – | 120 ($\tau_f^C$) | $7.6\times10^9$ | 0.91 | – | $8.6\times10^6$ (1020 nm) | 120 |
| (ZnP)$_2$–OxP | DCB | 80 | $1.2\times10^{10}$ | 0.96 | 0.58 | 83 ($\tau_f^O$) | | | | | |
| | toluene | 104 | $1.0\times10^{10}$ | 0.95 | – | 118 ($\tau_f^O$) | | | | | |
| (C$_{60}$Im:ZnP)$_2$–OxP | DCB | <10 | $>1.0\times10^{11}$ | 0.99 | 0.73[f] (0.66)[g] | 160 ($\tau_f^C$) | $5.5\times10^9$ | 0.89 | 0.35[g] | $1.1\times10^7$ (1020 nm) | 90 |
| | | | | | | | | | | $1.4\times10^7$ (840 nm) | 70 |
| | toluene | <10 | $>1.0\times10^{11}$ | 0.99 | – | 190 ($\tau_f^C$) | $4.6\times10^9$ | 0.86 | – | $8.7\times10^6$ (1020 nm) | 120 |

[a] Fluorescence lifetime $(\tau_f)_{sample}$ for major short component, and $(\tau_f)_{ref}$ of the reference compound ZnP was evaluated to be 1900 ps in DCB and 2000 ps in toluene. The quenching rate constant ($k_q$) and quenching quantum yield ($\Phi_q$) values of $^1$ZnP* and $^1$C$_{60}$* were calculated as follows: $k_q = (1/\tau_f)_{sample} - (1/\tau_f)_{ref}$; $\Phi_q = \frac{(1/\tau_f)_{sample} - (1/\tau_f)_{ref}}{(1/\tau_f)_{sample}}$. [b] Free energies of charge separation ($\Delta G_{CS}$) were calculated from $\Delta G_{CS} = E_{Ox} - E_{Red} - \Delta E_{0\text{-}0} + \Delta G_S$, in which $\Delta G_S = \frac{e^2}{4\pi\varepsilon_0\varepsilon_R R_{CC}}$, by using $\Delta E_{0\text{-}0} = 2.07$ eV for $^1$ZnP* and 1.75 eV for $^1$C$_{60}$*, $E_{Ox} = 0.28$ V for ZnP, and $E_{Red} = -1.29$ V for OxP vs. Fc/Fc$^+$ in DCB. $R_{CC} = 11.8$ Å, for (ZnP)$_2$–OxP. Permittivities of toluene and DCB are 2.38 and 9.93, respectively. [c] From the decay rate at 1000 nm. [d] Charge separation rate constant ($k_{CS}$). [e] Lifetime of radical ion pair ($\tau_{RIP}$). [f] For (ZnP$^{\bullet+}$)–OxP$^{\bullet-}$ and (ZnP$^{\bullet+}$:ImC$_{60}$)–OxP$^{\bullet-}$ etc. [g] For (ZnP$^{\bullet+}$:ImC$_{60}^{\bullet-}$)–OxP etc.

$\Phi_q^{C,O}$ values are in the range of 0.85–0.95 (Table 1). Both $k_q^{C,O}$ and $\Phi_q^{C,O}$ values tend to increase when going from the pentad to the triad. Furthermore, these values increase with increasing solvent polarity, which suggests the occurrence of competitive charge-separation and energy-transfer processes. To distinguish between these two quenching mechanisms, nanosecond transient absorption spectral measurements on the triad and the pentad were performed to characterize the charge-separation products.

Nanosecond transient absorption spectra for $(C_{60}Im:ZnP)_2$–OxP in DCB (Figure 7) were obtained through excitation by using laser light ($\lambda = 532$ nm). Broad

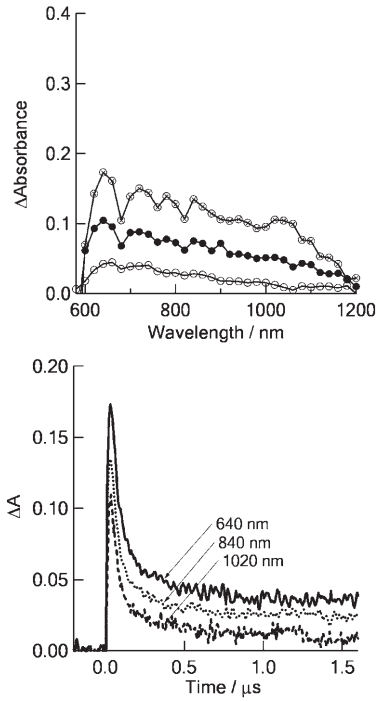


Figure 7. a) Nanosecond transient absorption spectra of $(C_{60}Im:ZnP)_2$–OxP ([component] = 0.07 mM) observed by means of laser irradiation at 532 nm in at 30 ns (⊗), 0.1 μs (●) and 1.0 μs (○) in DCB. b) Absorption-time profiles for the peaks in a) at the wavelengths indicated.

absorption bands were observed in the $\lambda = 600$–1200 nm region in which a band in the $\lambda = 600$–700 nm region was attributed to the $ZnP^{\bullet+}$ moiety, a band at $\lambda = 700$–900 nm was attributed to $OxP^{\bullet-}$ (see the Supporting Information), and a band at around $\lambda = 1020$ nm was attributed to $C_{60}^{\bullet-}$. Thus, these absorptions may include two radical ion pairs, $(C_{60}Im:ZnP)(ZnP^{\bullet+}:ImC_{60}^{\bullet-})$–OxP and $(C_{60}Im:ZnP)(ZnP^{\bullet+}:ImC_{60})$–$OxP^{\bullet-}$, which suggest that charge separation between ZnP and $C_{60}$, and a competitive charge-separation process between ZnP and OxP occur. Similar transient absorption spectral behavior was observed for triad $(C_{60}Im:ZnP)$–OxP. From the decay–time profiles in Figure 7b, the charge-recombination rate constants ($k_{CR}$) were evaluated. The decay of $C_{60}^{\bullet-}$ at $\lambda = 1020$ nm was faster than that of $OxP^{\bullet-}$ at $\lambda = 840$ nm, which results in $k_{CR}$ values of $1.4\times10^7\ s^{-1}$ and $1.1\times10^7\ s^{-1}$, respectively. For $(C_{60}Im:ZnP)$–OxP in DCB, only decay at $\lambda = 1020$ nm was observed. In toluene, the transient absorption band appeared at $\lambda = 1020$ nm as a shoulder of the main triplet absorption bands in the $\lambda = 650$–800 nm region for both $(C_{60}Im:ZnP)_n$–OxP complexes, whereas no near-IR band was observed for the $(ZnP)_n$–OxP compounds. These results suggest that charge-separation takes place to generate $(ZnP^{\bullet+}:ImC_{60}^{\bullet-})$–OxP for the supramolecular triad, and $(C_{60}Im:ZnP)(ZnP^{\bullet+}:ImC_{60}^{\bullet-})$–OxP for the supramolecular pentad. By using the $k_{CS}$ and $k_{CR}$ values obtained, the $k_{CS}/k_{CR}$ ratios were evaluated as a measure of the extent of charge stabilization in the photoinduced charge-separation process. These values were approximately 100, which demonstrates that there is some charge stabilization in the supramolecular triad and the pentad.

Figure 8 shows the energy-level diagram for the different photochemical events that occur in the triad. The energy levels of the charge-separated states were evaluated by

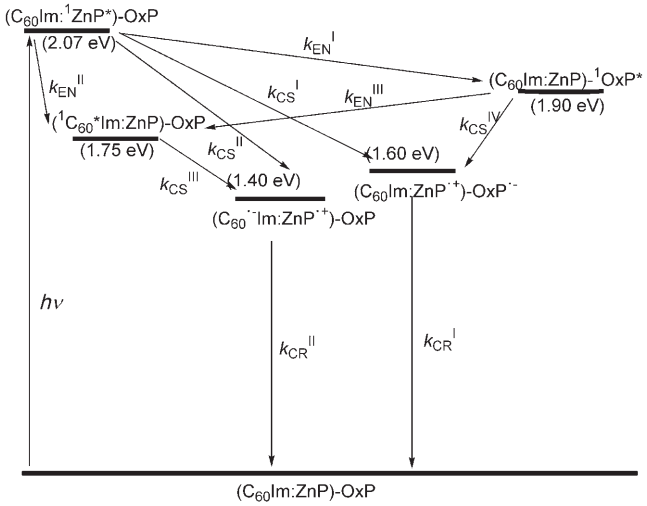


Figure 8. Energy level diagram that shows the different photochemical events for $(C_{60}Im:ZnP)$–OxP in DCB.

using the Rehm–Weller approach discussed earlier. Although the photochemical events of the supramolecular complexes in Figure 8 seem complex, it was possible to dissect the different photochemical pathways and evaluate the rate constants with reasonably good accuracy. The emission and transient absorption studies demonstrated that upon excitation of the ZnP entity of $(C_{60}Im:ZnP)$–OxP in toluene, energy transfer from the ZnP singlet-excited state to OxP is the predominant photoinduced process ($k_{EN}^{I}$ in Figure 8) and the anticipated charge-separation process is not appreciable. The $k_{EN}^{I}$ value was found to be $6.3\times10^9\ s^{-1}$ from the $k_q^Z$ of ZnP–OxP in toluene (Table 1). From the difference between the $k_{EN}^{I}$ value and the $k_q^Z$ value of $1.0\times10^{10}\ s^{-1}$ for $(C_{60}Im:ZnP)$–OxP, the sum of the energy transfer and charge separation from the ZnP singlet-excited state to $C_{60}$ ($k_{EN}^{II}+k_{CS}^{II}$) was found to be $3.7\times10^9\ s^{-1}$ in toluene. However, in polar DCB, a charge-separation process predominates.

  

The $k_{CS}^{I}$ value for the generation of $(C_{60}Im:ZnP^{\bullet+})$–$OxP^{\bullet-}$ was found to be $3.0\times10^{9}\,s^{-1}$, as estimated from the difference between the $k_q^Z$ value for ZnP–OxP and the $k_{EN}^{I}$ value. The $k_{CS}^{II}$ value for $(C_{60}^{\bullet-}Im:ZnP^{\bullet+})$–OxP, which is formed via $^1$ZnP*, was found to be $2.0\times10^{9}\,s^{-1}$, as estimated from the difference between the $k_q^Z$ values for $(C_{60}Im:ZnP)$–OxP and ZnP–OxP in DCB.

For $(ZnP)_n$–OxP in toluene, the $k_q^O$ values can be attributed to the energy transfer from $^1$OxP* to ZnP ($k_{EN}^{III}$), whereas in DCB they are ascribed to charge separation via $^1$OxP* to generate $(ZnP^{\bullet+})$–$OxP^{\bullet-}$ ($k_{CS}^{IV}$). For $(C_{60}Im:ZnP)_n$–OxP in toluene, the $k_q^{C,O}$ value is larger than that for $(ZnP)_n$–OxP (the $k_q^{C,O}$ value must be $k_q^C$), which can be assigned to the energy transfer from $^1$OxP* to $C_{60}$ ($k_{EN}^{III}$). In DCB, the $k_q^{C,O}$ value of $(C_{60}Im:ZnP)$–OxP must be $k_q^C$; this quenching rate constant can be associated with the $k_{CS}^{III}$ value, which describes the formation of $(C_{60}^{\bullet-}Im:ZnP^{\bullet+})$–OxP from $^1C_{60}$*.

For the charge-recombination processes of $(C_{60}Im:ZnP)_2$–OxP in DCB, the $k_{CR}$ value ($1.1\times10^{7}\,s^{-1}$) evaluated from the decay of $OxP^{\bullet-}$ can be assigned to $k_{CR}^{I}$, whereas the $k_{CR}$ value ($1.4\times10^{7}\,s^{-1}$) evaluated from the decay of $C_{60}^{\bullet-}$ can be assigned to $k_{CR}^{II}$. Intramolecular electron mediation from $OxP^{\bullet-}$ to $C_{60}$ is considered to be slow as a result of the long distance ($\approx$15 Å) between these entities.

## Conclusions

We have successfully assembled novel supramolecular pentads and triads composed of zinc–porphyrin(s), fullerene(s), and oxoporphyrinogen donor–acceptor entities by using a covalent-coordinate bonding approach. The supramolecular structures were fully characterized by means of spectral, computational, and electrochemical techniques. As predicted from the free-energy calculations, photoinduced electron transfer from the porphyrin singlet-excited state to the fullerene entity in DCB was demonstrated by means of time-resolved emission and transient absorption studies. The experimentally measured charge-separation rates ($k_{CS}$) were higher for pentad $(C_{60}Im:ZnP)_2$–OxP than those of the corresponding triad, $C_{60}$Im:ZnP–OxP. The lifetimes of the radical ion pair ($\tau_{RIP}$) were found to be about 100 ns, which indicates some degree of charge stabilization in the supramolecular systems we have studied. The results reveal that some modulation of the porphyrin–fullerene energy/electron-transfer processes can be achieved through careful design of the polychromophoric system. We are currently attempting to further influence the intramolecular energy and electronic processes through the introduction of inorganic cofactors, which can be appended to the triad or the pentad by means of hydrogen bonds at the opposing face of the porphyrinogen moiety.[23]

## Experimental Section

**Chemicals**: All solvents and reagents were used as received. Reactions were performed under an atmosphere of dry nitrogen. Size-exclusion chromatography was performed by using Biorad BioBeads SX-1. Tetra-*n*-butylammonium perchlorate was obtained from Fluka Chemicals. Syntheses of $ImC_{60}$ and $(ZnP)_2$–OxP were carried out according to literature procedures.[15–16]

**ZnP–OxP**: Tetrakis(3,5-di-*t*-butyl-4-oxocyclo-hexadien-2,5-ylidene)porphyrinogen[18] (100 mg, $9.0\times10^{-5}$ mol) and 5-(4-bromomethylphenyl)-10,15,20-triphenylporphinato zinc(II)[15] (70 mg, $9.1\times10^{-5}$ mol) were dissolved in dry *N*,*N*-dimethylformamide (5 mL) before anhydrous potassium carbonate (200 mg) was added. The mixture was stirred at 80 °C for 3–4 h until consumption of porphyrinyl benzyl bromide was observed by means of thin-layer chromatography. The reaction mixture was poured into water and then extracted with dichloromethane ($2\times30$ mL). The combined organic fractions were dried over anhydrous sodium sulfate, filtered, and the solvent was removed under reduced pressure. The product was purified by means of column chromatography using a silica gel column with dichloromethane/hexane (50:50 to 100:0) as the eluent. The ZnP–OxP dyad was collected as the fraction that elutes prior to that of the parent porphyrinogen (final fraction). Further purification was affected by means of size-exclusion chromatography with tetrahydrofuran as the eluent (61 mg, 26%). $^1$H NMR (300 MHz, $CDCl_3$, 25 °C, TMS): $\delta=$ 1.12 (s, 36H; $-C(CH_3)_3$), 1.35, 1.37, 1.39 ($3\times$s, 54H; $-C(CH_3)_3$), 4.68 (s, 2H; benzylic $CH_2$), 6.76 (s, 2H; cyclohexadienyl–*H*), 6.81 (d, $J=$ 2.204 Hz, 2H; cyclohexadienyl–*H*), 6.90–7.10 (m, 6H; cyclohexadienyl–*H* (4H), porphyrinogen β-pyrrolic–*H* (2H)), 7.42, 7.48, 7.57 ($3\times$d, $J=$ 2.204 Hz, 2H; porphyrinogen β-pyrrolic–*H*), 7.75 (m, 11H; phenyl–*H*), 7.99 (d, $J=8.08$ Hz, 2H; phenyl–*H*), 8.16 (m, 6H; phenyl–*H*), 8.41 (d, $J=4.77$ Hz, 2H; porphyrinic β-pyrrolic–*H*), 8.6 (brs, 1H; N*H*), 8.80 (d, $J=4.77$ Hz, 2H; porphyrinic β-pyrrolic–*H*), 8.94 (m, 4H; porphyrinic β-pyrrolic–*H*), 9.34 ppm (brs, 2H; N*H*); $^{13}$C NMR (75 MHz, $CDCl_3$): $\delta=$ 29.40, 29.47, 29.51, 29.57, 35.40, 35.51, 35.60, 35.74, 118.76, 119.31, 119.80, 119.95, 121.06, 121.39, 124.38, 126.56, 126.59, 126.62, 127.54, 130.87, 131.17, 131.54, 131.58, 131.60, 131.79, 132.09, 132.18, 132.49, 133.93, 134.27, 134.29, 134.33, 134.36, 134.38, 135.87, 136.63, 136.98, 142.46, 147.59, 147.67, 147.83, 148.77, 149.69, 150.17, 150.24, 150.25, 185.77, 185.96 ppm. MALDI-TOF (dithranol): $m/z$: 1816 ($[M+3H]^+$).

**Instrumentation**: $^1$H and $^{13}$C NMR spectra were obtained by using a JEOL AL300BX NMR spectrometer with tetramethylsilane as the internal standard in $CDCl_3$ solutions. MALDI-TOF mass spectroscopy was performed by using a Shimadzu instrument. The UV-visible spectral measurements were carried out by using a Shimadzu Model 1600 UV-visible spectrophotometer. The fluorescence emission was monitored by using a Spex Fluorolog-tau spectrometer. Cyclic voltammograms were recorded by using an EG&G Model 263 A potentiostat with a three electrode system. A platinum button or glassy carbon electrode was used as the working electrode. A platinum wire served as the counter electrode and Ag/AgCl was used as the reference electrode. The ferrocene/ferrocenium redox couple was used as an internal standard. All the solutions were purged prior to electrochemical and spectral measurements by using argon gas. The computational calculations were performed by means of DFT B3LYP/3-21G(*) methods with GAUSSIAN 03 software package[20] by using high speed computers.

**Time-resolved emission and transient absorption measurements**: Picosecond time-resolved fluorescence spectra were measured by using an argon ion pumped Ti/sapphire laser (Tsunami; pulse width = 2 ps) and a streak scope (Hamamatsu Photonics; response time = 10 ps). The details of the experimental setup are described elsewhere.[24] Nanosecond transient absorption spectra in the NIR region were measured by means of laser-flash photolysis in which light from an Nd/YAG laser ($\lambda=532$ nm; pulse width = 6 ns) was used as the excitation source and a Ge-avalanche-photodiode module was used for detecting the monitoring light from a pulsed Xe lamp for shorter timescale measurements than 5 μs. For timescale measurements longer than 5 μs, the InGaAs photodiode detector was used to detect the monitoring light from the continuous Xe lamp.[24]

## Acknowledgements

This work is supported by the National Science Foundation (grant 0453464 to F.D.), the donors of the Petroleum Research Fund administered by the American Chemical Society, and Grants-in-Aid for Scientific Research on Primary Area (417 (to O.I. and Y.A.)) and a Priority Area "Super-Hierarchical Structures (to J.P.H. and K.A.)" from the Ministry of Education, Culture, Sports, Science and Technology, Japan.

[1] a) R. A. Marcus, N. Sutin, *Biochim. Biophys. Acta* **1985**, *811*, 265; b) R. A. Marcus, *Angew. Chem.* **1993**, *105*, 1161; *Angew. Chem. Int. Ed. Engl.* **1993**, *32*, 1111; c) M. Bixon, J. Jortner, *Adv. Chem. Phys.* **1999**, *106*, 35.

[2] a) J. R. Winkler, H. B. Gray, *Chem. Rev.* **1992**, *92*, 369; b) C. Kirmaier, D. Holton in *The Photosynthetic Reaction Center, Vol. II* (Eds.: J. Deisenhofer, J. R. Norris), Academic Press, San Diego, **1993**, pp. 49–70.

[3] a) G. McLendon, R. Hake, *Chem. Rev.* **1992**, *92*, 481; b) I. R. Gould, S. Farid, *Acc. Chem. Res.* **1996**, *29*, 522; c) N. Mataga, H. Miyasaka, *Adv. Chem. Phys.* **1999**, *107*, 431; d) F. D. Lewis, R. L. Letsinger, M. R. Wasielewski, *Acc. Chem. Res.* **2001**, *34*, 159.

[4] a) J. R. Miller, L. T. Calcaterra, G. L. Closs, *J. Am. Chem. Soc.* **1984**, *106*, 3047; b) G. L. Closs, J. R. Miller, *Science* **1988**, *240*, 440; c) J. S. Connolly, J. R. Bolton in *Photoinduced Electron Transfer, Part D* (Eds.: M. A. Fox, M. Chanon), Elsevier, Amsterdam, **1988**, pp. 303–393.

[5] a) M. R. Wasielewski, *Chem. Rev.* **1992**, *92*, 435; b) H. Kurreck, M. Huber, *Angew. Chem.* **1995**, *107*, 929; *Angew. Chem. Int. Ed. Engl.* **1995**, *34*, 849; c) D. Gust, T. A. Moore, A. L. Moore, *Acc. Chem. Res.* **2001**, *34*, 40.

[6] a) A. Harriman, J.-P. Sauvage, *Chem. Soc. Rev.* **1996**, *25*, 41; b) M.-J. Blanco, M. C. Jiménez, J.-C. Chambron, V. Heitz, M. Linke, J.-P. Sauvage, *Chem. Soc. Rev.* **1999**, *28*, 293; c) V. Balzani, A. Juris, M. Venturi, S. Campagna, S. Serroni, *Chem. Rev.* **1996**, *96*, 759; d) *Electron Transfer in Chemistry* (Ed.: V. Balzani), Wiley-VCH, Weinheim, **2001**.

[7] a) M. N. Paddon-Row, *Acc. Chem. Res.* **1994**, *27*, 18; b) J. W. Verhoeven, *Adv. Chem. Phys.* **1999**, *106*, 603; c) K. Maruyama, A. Osuka, N. Mataga, *Pure Appl. Chem.* **1994**, *66*, 867; d) A. Osuka, N. Mataga, T. Okada, *Pure Appl. Chem.* **1997**, *69*, 797; e) *Molecular Catenanes, Rotaxanes and Knots* (Eds.: J.-P. Sauvage, C. Dietrich-Buchecker), Wiley-VCH, Weinheim, **1999**.

[8] a) J. S. Sessler, B. Wang, S. L. Springs, C. T. Brown in *Comprehensive Supramolecular Chemistry* (Eds.: J. L. Atwood, J. E. D. Davies, D. D. MacNicol, F. Vögtle), Pergamon, Oxford, **1996**, Chapter 9; b) T. Hayashi, H. Ogoshi, *Chem. Soc. Rev.* **1997**, *26*, 355; c) M. W. Ward, *Chem. Soc. Rev.* **1997**, *26*, 365.

[9] a) *Introduction of Molecular Electronics* (Eds.: M. C. Petty, M. R. Bryce, D. Bloor), Oxford University Press, New York, **1995**; b) *Molecular Switches* (Ed.: B. L. Feringa), Wiley-VCH, Weinheim, **2001**.

[10] a) J. S. Connolly, J. R. Bolton in *Photoinduced Electron Transfer, Part D* (Eds.: M. A. Fox, M. Chanon), Elsevier, Amsterdam, **1988**, pp. 303–393; b) D. M. Guldi, N. Martin, *J. Mater. Chem.* **2002**, *12*, 1978; c) L. Sanchez, N. Martin, D. M. Guldi, *Angew. Chem.* **2005**, *117*, 5508; *Angew. Chem. Int. Ed.* **2005**, *44*, 5374.

[11] D. Gust, T. A. Moore in *The Porphyrin Handbook, Vol. 8* (Ed.: K. M. Kadish, K. M. Smith, R. Guilard), Academic Press, Burlington, **2000**, pp. 153–190.

[12] a) K. M. Kadish, R. S. Ruoff, *Fullerenes: Chemistry, Physics, and Technology*, Wiley-VCH, Weinheim, **2000**; b) H. Imahori, Y. Sakata, *Adv. Mater.* **1997**, *9*, 537; c) M. Prato, *J. Mater. Chem.* **1997**, *7*, 1097; d) N. Martín, L. Sánchez, B. Illescas, I. Pérez, *Chem. Rev.* **1998**, *98*, 2527; e) F. Diederich, M. Gómez-López, *Chem. Soc. Rev.* **1999**, *28*, 263; f) D. M. Guldi, *Chem. Commun.* **2000**, 321; g) D. M. Guldi, M. Prato, *Acc. Chem. Res.* **2000**, *33*, 695; h) D. M. Guldi, *Chem. Soc. Rev.* **2002**, *31*, 22; i) M. D. Meijer, G. P. M. van Klink, G. van Koten, *Coord. Chem. Rev.* **2002**, *230*, 141; j) M. E. El-Khouly, O. Ito, P. M. Smith, F. D'Souza, *J. Photochem. Photobiol. C* **2004**, *5*, 79; k) H. Imahori, S. Fukuzmi, *Adv. Funct. Mater.* **2004**, *14*, 525; l) F. D'Souza, O. Ito, *Coord. Chem. Rev.* **2005**, *249*, 1410; m) I. Bouamaied, T. Coskun, E. Stulz, *Struct. Bonding* **2006**, *121*, 1.

[13] a) H. W. Kroto, J. R. Heath, S. C. O'Brien, R. F. Curl, R. E. Smalley, *Nature* **1985**, *318*, 162; b) W. Kratschmer, L. D. Lamb, F. Fostiropoulos, D. R. Huffman, *Nature* **1990**, *347*, 345.

[14] a) *Fullerene and Related Structures, Vol. 199* (Ed.: A. Hirsch), Springer, Berlin, **1999**; b) Q. Xie, E. Pèrez-Cordero, L. Echegoyen, *J. Am. Chem. Soc.* **1992**, *114*, 3978; c) H. Imahori, K. Hagiwara, T. Akiyama, M. Akoi, S. Taniguchi, T. Okada, M. Shirakawa, Y. Sakata, *Chem. Phys. Lett.* **1996**, *263*, 545; d) D. M. Guldi, K.-D. Asmus, *J. Am. Chem. Soc.* **1997**, *119*, 5744; e) H. Imahori, M. E. El-Khouly, M. Fujitsuka, O. Ito, Y. Sakata, S. Fukuzumi, *J. Phys. Chem. A* **2001**, *105*, 325.

[15] J. P. Hill, A. S. D. Sandanayaka, A. L. McCarty, P. A. Karr, M. E. Zandler, R. Charvet, K. Ariga, Y. Araki, O. Ito, F. D'Souza, *Eur. J. Org. Chem.* **2006**, 595.

[16] F. D'Souza, G. R. Deviprasad, M. E. Zandler, V. T. Hoang, K. Arkady, M. VanStipdonk, A. Perera, M. E. El-Khouly, M. Fujitsuka, O. Ito, *J. Phys. Chem. A* **2002**, *106*, 3243.

[17] H. A. Benesi, J. H. Hildebrand, *J. Am. Chem. Soc.* **1949**, *71*, 2703.

[18] a) J. P. Hill, I. J. Hewitt, C. E. Anson, A. K. Powell, A. L. McCarty, P. A. Karr, M. E. Zandler, F. D'Souza, *J. Org. Chem.* **2004**, *69*, 5861; b) J. P. Hill, W. Schmitt, A. L. McCarty, K. Ariga, F. D'Souza, *Eur. J. Org. Chem.* **2005**, 2893.

[19] a) D. Rehm, A. Weller, *Isr. J. Chem.* **1970**, *8*, 259; b) N. Mataga, H. Miyasaka in *Electron Transfer, Part 2* (Eds.: J. Jortner, M. Bixon), Wiley, New York, **1999**, pp. 431.

[20] Gaussian 03, Revision B.04, M. J. Frisch, G. W. Trucks, H. B. Schlegel, G. E. Scuseria, M. A. Robb, J. R. Cheeseman, J. A. Montgomery, Jr., T. Vreven, K. N. Kudin, J. C. Burant, J. M. Millam, S. S. Iyengar, J. Tomasi, V. Barone, B. Mennucci, M. Cossi, G. Scalmani, N. Rega, G. A. Petersson, H. Nakatsuji, M. Hada, M. Ehara, K. Toyota, R. Fukuda, J. Hasegawa, M. Ishida, T. Nakajima, Y. Honda, O. Kitao, H. Nakai, M. Klene, X. Li, J. E. Knox, H. P. Hratchian, J. B. Cross, V. Bakken, C. Adamo, J. Jaramillo, R. Gomperts, R. E. Stratmann, O. Yazyev, A. J. Austin, R. Cammi, C. Pomelli, J. W. Ochterski, P. Y. Ayala, K. Morokuma, G. A. Voth, P. Salvador, J. J. Dannenberg, V. G. Zakrzewski, S. Dapprich, A. D. Daniels, M. C. Strain, O. Farkas, D. K. Malick, A. D. Rabuck, K. Raghavachari, J. B. Foresman, J. V. Ortiz, Q. Cui, A. G. Baboul, S. Clifford, J. Cioslowski, B. B. Stefanov, G. Liu, A. Liashenko, P. Piskorz, I. Komaromi, R. L. Martin, D. J. Fox, T. Keith, M. A. Al-Laham, C. Y. Peng, A. Nanayakkara, M. Challacombe, P. M. W. Gill, B. Johnson, W. Chen, M. W. Wong, C. Gonzalez, J. A. Pople, Gaussian, Inc., Wallingford CT, **2004**.

[21] For examples of B3LYP/3-21G(*) applied to porphyrin–fullerene systems, see: M. E. Zandler, F. D'Souza, *C. R. Chim.* **2006**, *9*, 960.

[22] a) T. Nojiri, A. Watanabe, O. Ito, *J. Phys. Chem. A* **1998**, *102*, 5215; b) H. N. Ghosh, H. Pal, A. V. Sapre, J. P. Mittal, *J. Am. Chem. Soc.* **1993**, *115*, 11722; c) M. Fujitsuka, O. Ito, T. Yamashiro, Y. Aso, T. Otsubo, *J. Phys. Chem. A* **2000**, *104*, 4876; d) F. D'Souza, P. M. Smith, M. E. Zandler, A. L. McCarty, M. Itou, Y. Araki, O. Ito, *J. Am. Chem. Soc.* **2004**, *126*, 7898.

[23] J. P. Hill, A. L. Schumacher, F. D'Souza, J. Labuta, C. Redshaw, M. J. R. Elsegood, M. Aoyagi, T. Nakanishi, K. Ariga, *Inorg. Chem.* **2006**, *45*, 8288.

[24] a) K. Matsumoto, M. Fujitsuka, T. Sato, S. Onodera, O. Ito, *J. Phys. Chem. B* **2000**, *104*, 11632; b) S. Komamine, M. Fujitsuka, O. Ito, K. Morikawa, T. Miyata, T. Ohno, *J. Phys. Chem. A* **2000**, *104*, 11497; c) M. Yamazaki, Y. Araki, M. Fujitsuka, O. Ito, *J. Phys. Chem. A* **2001**, *105*, 8615.

Received: December 21, 2006
Published online: March 27, 2007

  